

# Structure Preserving Model Order Reduction of Shallow Water Equations

Bülent Karasözen<sup>a,b,\*</sup>, Süleyman Yıldız<sup>a</sup>, Murat Uzunca<sup>c</sup>

<sup>a</sup>*Institute of Applied Mathematics, Middle East Technical University, Ankara, Turkey*

<sup>b</sup>*Department of Mathematics, Middle East Technical University, Ankara, Turkey*

<sup>c</sup>*Department of Mathematics, Sinop University, Sinop, Turkey*

---

## Abstract

The two-dimensional rotational shallow water equations (SWEs) in the non-canonical Hamiltonian/Poisson form are integrated in time by the fully implicit average vector field (AVF) method, and in the f-plane as a partial differential equation (PDE) with quadratic nonlinearity by the linearly implicit Kahan's method. Reduced order models (ROMs) with proper orthogonal decomposition/discrete empirical interpolation method (POD/DEIM) preserve the Hamiltonian structure, and the tensorial POD the linear-quadratic structure of the SWE in the f-plane. We show that both methods preserve numerically the invariants like energy, the Casimirs like the enstrophy, mass, and circulation over a long time. The accuracy and computational efficiency of the ROMs are shown in numerical test problem.

*Keywords:* Finite difference methods, linearly implicit methods, preservation of invariants, proper orthogonal decomposition, discrete empirical interpolation, tensorial proper orthogonal decomposition.

*2010 MSC:* 65P10, 65M60,

---

## 1. Introduction

The shallow water equations (SWEs) consist of a set of two-dimensional equations describing a thin inviscid fluid layer flowing over the topography in a frame rotating about an arbitrary axis. SWEs are widely used in modeling of large-scale atmosphere/ocean dynamics, in numerical weather prediction. Energy and enstrophy are the most important conserved quantities of the SWEs, whereas the energy cascades to large scales whilst enstrophy cascades to small scales [1, 2]. Therefore numerical schemes that preserve energy and enstrophy lead to stable solutions in long term integration. Salmon [3] introduced the

---

\*Corresponding author

Email addresses: [bulent@metu.edu.tr](mailto:bulent@metu.edu.tr) (Bülent Karasözen),  
[yildiz.suleyman@metu.edu.tr](mailto:yildiz.suleyman@metu.edu.tr) (Süleyman Yıldız), [muzunca@sinop.edu.tr](mailto:muzunca@sinop.edu.tr) (Murat Uzunca)

non-canonical Hamiltonian/Poisson form of the SWE in the rotation frame with constant Coriolis force and constructed an energy preserving scheme in space using Arakawa-Lambs discretization [4]. The SWEs with the complete Coriolis force are introduced in [5] and share the same continuous skew-symmetric structure and Poisson bracket. The discrete energy conservation follows from antisymmetry of the discrete Poisson bracket, other conserved quantities are potential enstrophy, mass and vorticity, i.e. the Casimirs.

Time discretization schemes that preserve geometric structure like the symplecticness, energy or entropy lead to stable approximate solutions of dynamical systems in long time integration [6, 7]. In this paper, we discretize SWE using finite differences in space by preserving the skew-symmetry Poisson matrix. We apply two different time discretization methods for the semi-discretized SWE. The first one is the energy preserving fully implicit, second order convergent average vector field (AVF) method [8, 9]. The AVF method belongs to the class of the discrete gradient method for ODEs [10, 11, 12]. Alternatively the semi-discretization of the SWE in the f-plane form leads to system of ordinary differential equations (ODEs) with quadratic nonlinearities. We use second order linearly implicit Kahan's method [13] for time integration. SWE in the f-plane [14] is a linear-quadratic ordinary differential equation (ODE) after semi-discretization by finite differences in space. Kahan's "unconventional" discretization method applied to ODEs with quadratic vector fields, preserves the integrals or conserved quantities of many Hamiltonian and integrable systems. Fully implicit schemes like the AVF method require iterative solvers like Newton's method at each time step for solving the nonlinear systems. Linearly implicit schemes like Kahan's method require the solution of precisely one linear system of equations in each time step.

Numerical methods for solving partial differential equations (PDEs) are computationally costly and require a large amount of computer memory for applications in real-time or for evaluations for many different parameters. During the last decades, reduced order methods (ROMs) have emerged as a powerful approach to reduce the cost of evaluating large systems of PDEs by constructing a low-dimensional linear reduced subspace, that approximately represents the solution to the system of PDEs with a significantly reduced computational cost. The proper orthogonal decomposition (POD) with the Galerkin projection into lower dimensional space, has been widely used as a computationally efficient surrogate model in large-scale numerical simulations of nonlinear PDEs. The high fidelity solutions are generated by numerical simulations of the discretized high dimensional full order model (FOM). The POD is then applied with the Galerkin projection to compute an optimal subspace to fit the high fidelity data. In the online stage, the reduced system is solved in the low-dimensional subspace. The primary challenge in producing the low dimensional models of the high dimensional discretized PDEs is the efficient evaluation of the nonlinearities (inner products) on the POD basis. The computational cost is reduced by sampling the nonlinear terms and interpolating, known as hyper-reduction techniques. Several hyper-reduction methods are developed to reduce the computational cost of evaluating the reduced nonlinear terms, empirical interpolation method

(EIM) [15], discrete empirical interpolation method (DEIM) [16], missing point estimation [17, 18], best points interpolation [19], gappy POD [20]. We use DEIM, which is one of the most frequently used hyper-reduction methods. Rigorous error and stability analysis are in general not amenable for subsampling procedures used in hyper-reduction methods. For PDEs and ODEs with polynomial nonlinearities, ROMs do not require approximating the nonlinear terms through sampling, the reduced order operators can be precomputed. Projection of FOM onto the reduced space yields low-dimensional matrix operators that preserve the polynomial structure of the FOM. This is an advantage because the offline-online computation is separated in contrast to the hyper-reduction methods. For polynomial nonlinearities, tensorial POD preserve the structure of FOM in the reduced space. Recently, tensorial POD methods are applied for PDEs and ODEs with polynomial nonlinearities [21, 22, 23, 24, 25].

The naive application of POD/DEIM and tensorial POD may not preserve the geometric structures, like the symplecticness, energy preservation and passivity of Hamiltonian, Lagrangian and port Hamiltonian PDEs. The stability of reduced models over long-time integration and the structure-preserving properties has been recently investigated in the context of Lagrangian systems [26, 27], and for port-Hamiltonian systems [28]. For linear and nonlinear Hamiltonian systems, the symplectic model reduction technique, proper symplectic decomposition (PSD) is constructed for Hamiltonian systems like, linear wave equation, sine-Gordon equation, nonlinear Schrödinger (NLS) equation to ensure long term stability of the reduced model [29, 30]. Recently the AVF method is used as a time integrator to construct reduced order models for Hamiltonian systems like Korteweg-de Vries equation [31] and NLS equation [32]. Reduced order models for the SWEs are constructed in conservative form using POD-DEIM [33, 34], in the  $\beta$ -plane by POD-DEIM and tensorial POD [35, 36], by dynamic mode decomposition (DMD) [37, 38], the f-plane using POD [39]. In these articles, the preservation of the energy and other conservative quantities in the reduced space are not discussed. We apply the POD/DEIM for the SWE in Poisson form and integrate in time using the AVF method which preserves the Hamiltonian (energy) in the reduced space. Using the quadratic semi-discretized form of the SWE in the f-plane, we also apply two different tensorial POD algorithms [21, 22, 23] using the matricization of tensor and exploiting the sparse structure of the discretized SWE. The reduced equations are also solved by the linearly implicit Kahan's method. A comparison with DEIM shows the efficiency of the tensorial POD by exploiting the quadratic structure of the semi-discretized SWE.

In the next section, we introduce the SWE in Hamiltonian form and in the f-plane. The finite difference discretization in space and time integration by the AVF method and Kahan's method are presented in Section 3. POD/DEIM reduced models are constructed for the SWE in AVF semi-discretized Hamiltonian form, and tensorial POD for the semi-discrete ODE system with quadratic nonlinearities in Section 4. In Section 5, we compare POD, POD/DEIM, and tensorial POD for two dimensional rotating SWE with respect to the accuracy of the reduced solutions, preservation of the energy, enstrophy, vorticity and

computational efficiency by the ROMs. The paper ends with some conclusions.

## 2. Shallow water equation

Many geophysical flows can be written in Hamiltonian form [40]. The rotational SWE in non-canonical Hamiltonian/Poisson form was described in [3]. Later on the Nambu formulation of the SWE [41], SWE with complete Coriolis force [5, 2], and multi-layer SWE [2] are developed. The two-dimensional rotational SWE is given as [3]

$$\begin{aligned}\frac{\partial u}{\partial t} &= qhv - \Phi_x, \\ \frac{\partial v}{\partial t} &= -qhu - \Phi_y, \\ \frac{\partial h}{\partial t} &= -\frac{\partial}{\partial x}(hu) - \frac{\partial}{\partial y}(hv),\end{aligned}\tag{1}$$

where  $\mathbf{u}(\mathbf{x}, t) = (u(\mathbf{x}, t), v(\mathbf{x}, t))^T$  is the (particle) velocity,  $h(\mathbf{x}, t)$  is the fluid depth,  $q = (v_x - u_y + f)/h$  is the potential vorticity and  $f$  is the Coriolis force,  $g$  is the gravity constant,  $\mathbf{z} = (u, v, h)^T$  is the state vector and  $\mathbf{x} = (x, y)^T$ . The non-canonical Hamiltonian/Poisson form of the SWE (1) is given by

$$\frac{\partial \mathbf{z}}{\partial t} = \mathcal{J}(\mathbf{z}) \frac{\delta \mathcal{H}}{\delta \mathbf{z}} = \begin{pmatrix} 0 & q & -\partial_x \\ -q & 0 & -\partial_y \\ -\partial_x & -\partial_y & 0 \end{pmatrix} \begin{pmatrix} hu \\ hv \\ \frac{1}{2}(\mathbf{u} \cdot \mathbf{u}) + gh \end{pmatrix},\tag{2}$$

with the Hamiltonian (energy)

$$\mathcal{H} = \frac{1}{2} \iint h(\mathbf{u} \cdot \mathbf{u} + gh) d\mathbf{x}.\tag{3}$$

The skew-symmetric Poisson bracket is defined for any two functionals  $A$  and  $B$  [42, 3] as

$$\{A, B\} = \iint \left( q \frac{\delta((A, B)}{\delta(u, v)} - \frac{\delta A}{\delta \mathbf{u}} \cdot \nabla \frac{\delta B}{\delta h} + \frac{\delta B}{\delta \mathbf{u}} \cdot \nabla \frac{\delta A}{\delta h} \right) d\mathbf{x},\tag{4}$$

where  $\nabla = (\partial x, \partial y)$ , and  $\delta A / \delta \mathbf{u}$  is the functional derivative of  $A$  with respect to  $u$ . The functional Jacobian is given by

$$\frac{\delta((A, B)}{\delta(u, v)} = \frac{\delta A}{\delta u} \frac{\delta B}{\delta v} - \frac{\delta B}{\delta u} \frac{\delta A}{\delta v}.$$

The Poisson bracket (4) is related to the skew-symmetric Poisson matrix  $J$  as  $\{A, B\} = \{A, \mathcal{J}B\}$ . Although the matrix  $\mathcal{J}$  in (2) is not skew-symmetric, the skew-symmetry of the Poisson bracket appears after integrations by parts [42], and the Poisson bracket satisfies the Jacobi identity

$$\{A, \{B, C\}\} + \{B, \{C, A\}\} + \{A, \{B, C\}\}.$$

Conservation of the Hamiltonian (energy) (3) follows from the antisymmetry the Poisson bracket (4)

$$\frac{d\mathcal{H}}{dt} = \{\mathcal{H}, \mathcal{H}\} = 0.$$

Other conserved quantities are the Casimirs of the SWE [3] of the form

$$C = \iint hG(q)d\mathbf{x},$$

where  $G$  is an arbitrary function of the potential vorticity  $q$ . The Casimirs are additional constants of motion, they commute with all other state functions

$$\{F, C\} = 0, \quad \forall F(\mathbf{z}).$$

Important special cases are the potential enstrophy

$$\mathcal{Z} = \frac{1}{2} \iint hq^2 dx = \frac{1}{2} \iint \frac{1}{h} \left( \frac{\partial v}{\partial x} - \frac{\partial u}{\partial y} \right)^2 d\mathbf{x},$$

the mass  $\iint \mathbf{x}$ , and the vorticity  $\iint hq dx$ . Alternatively, inserting the potential vorticity  $q$  in (1), the SWE can be written in the f-plane as

$$\begin{aligned} \frac{\partial u}{\partial t} &= -uu_x - vu_y - gh_x + fv, \\ \frac{\partial v}{\partial t} &= -uv_x - vv_y - gh_y - fu, \\ \frac{\partial h}{\partial t} &= -(hu)_x - (hy)_x. \end{aligned} \tag{5}$$

### 3. Full order model (FOM)

We discretize the rotational SWE (1) using finite differences in a rectangular space domain  $\Omega = (a, b) \times (c, d)$  using the uniform grid  $(x_i, y_j) = (a + (i - 1)\Delta x, c + (j - 1)\Delta y)$ ,  $i = 1, \dots, n_x, j = 1, \dots, n_y$ . We take in both space direction the same mesh sizes  $\Delta x = \Delta y$ ,  $n_x = n_y$ . The matrix  $D$  denotes the first order central finite difference operators  $\partial_x$  and  $\partial_y$  under periodic boundary conditions

$$D = \begin{pmatrix} 0 & 1 & & & -1 \\ -1 & 0 & 1 & & \\ & \ddots & \ddots & \ddots & \\ & & -1 & 0 & 1 \\ 1 & & & 1 & 0 \end{pmatrix} \in \mathbb{R}^{n_x \times n_x}.$$

The corresponding first order finite difference approximations are  $D_x = \frac{1}{2\Delta x} D \otimes I_{n_x}$ ,  $D_y = \frac{1}{2\Delta y} I_{n_y} \otimes D$ , where  $\otimes$  denotes the Kronecker product. The identity

matrix of size  $s \times s$  is denoted by  $I_s$ . The semi-discrete form of (2) is given as

$$\frac{d\mathbf{z}}{dt} = J(\mathbf{z})\nabla H\mathbf{z} = \begin{pmatrix} 0 & \mathbf{q} & -D_x \\ -\mathbf{q} & 0 & -D_y \\ -D_x & -D_y & 0 \end{pmatrix} \begin{pmatrix} \mathbf{h} \circ \mathbf{u} \\ \mathbf{h} \circ \mathbf{v} \\ \frac{1}{2}(\mathbf{u} \circ \mathbf{u} + \mathbf{v} \circ \mathbf{v}) + g\mathbf{h} \end{pmatrix}, \quad (6)$$

where  $\circ$  denotes element-wise or Hadamard product. The discretized variables are

$$q_{i,j} \approx q(x_i, y_j), \quad u_{i,j} \approx u(x_i, y_j), \quad v_{i,j} \approx v(x_i, y_j), \quad h_{i,j} \approx h(x_i, y_j), \quad f_{i,j} \approx f(x_i, y_j),$$

and

$$\text{diag}(\mathbf{q}) = q_{i,j}, \quad \text{diag}(\mathbf{u}) = u_{i,j}, \quad \text{diag}(\mathbf{v}) = v_{i,j}, \quad \text{diag}(\mathbf{h}) = h_{i,j}, \quad \text{diag}(\mathbf{f}) = f_{i,j},$$

where  $\text{diag}$  denotes the diagonal vector and  $\mathbf{z} = (\mathbf{u}^T, \mathbf{v}^T, \mathbf{h}^T)^T$ .

Time integration of (6) by the average vector field (AVF) integrator [9] yields

$$\mathbf{z}^{n+1} = \mathbf{z}^n + \Delta t J \left( \frac{\mathbf{z}^{n+1} + \mathbf{z}^n}{2} \right) \int_0^1 \nabla \bar{H}(\xi(\mathbf{z}^{n+1} - \mathbf{z}^n) + \mathbf{z}^n) d\xi \quad (7)$$

where

$$J \left( \frac{\mathbf{z}^{n+1} + \mathbf{z}^n}{2} \right) = \begin{pmatrix} 0 & \bar{\mathbf{q}} & -D_x \\ \bar{\mathbf{q}} & 0 & -D_y \\ -D_x & -D_y & 0 \end{pmatrix},$$

$$\int_0^1 \nabla \bar{H}(\xi(\mathbf{z}^{n+1} - \mathbf{z}^n) + \mathbf{z}^n) d\xi = \begin{pmatrix} \frac{\mathbf{h}^{n+1} \circ \mathbf{u}^{n+1} + \mathbf{h}^n \circ \mathbf{u}^n}{2} + \frac{\mathbf{h}^{n+1} \circ \mathbf{u}^n + \mathbf{h}^n \circ \mathbf{u}^{n+1}}{6} \\ \frac{\mathbf{h}^{n+1} \circ \mathbf{v}^{n+1} + \mathbf{h}^n \circ \mathbf{v}^n}{3} + \frac{\mathbf{h}^{n+1} \circ \mathbf{v}^n + \mathbf{h}^n \circ \mathbf{v}^{n+1}}{6} \\ \frac{\mathbf{u}^{n+1} \circ \mathbf{u}^{n+1} + \mathbf{u}^{n+1} \circ \mathbf{u}^n + \mathbf{u}^n \circ \mathbf{u}^n}{6} + \frac{\mathbf{v}^{n+1} \circ \mathbf{v}^{n+1} + \mathbf{v}^{n+1} \circ \mathbf{v}^n + \mathbf{v}^n \circ \mathbf{v}^n}{6} + \frac{g(\mathbf{h}^{n+1} + \mathbf{h}^n)}{4} \end{pmatrix}.$$

The vorticity is discretized as

$$\bar{\mathbf{q}} = \frac{f - D_y \left( \frac{\mathbf{u}^{n+1} + \mathbf{u}^n}{2} \right) + D_x \left( \frac{\mathbf{v}^{n+1} + \mathbf{v}^n}{2} \right)}{\frac{\mathbf{h}^{n+1} + \mathbf{h}^n}{2}}$$

and  $\text{diag}(\bar{\mathbf{q}}) = \bar{q}_{i,j}$ ,  $i, j = 1, \dots, n_x$ . Discrete form of the conserved quantities are given by:

- energy

$$H = \frac{1}{2} \sum_{i,j} h_{i,j} (u_{i,j}^2 + v_{i,j}^2 + g h_{i,j}),$$

- potential enstrophy

$$Z = \frac{1}{2} \left( \frac{1}{2\Delta x} \right)^2 \sum_{i,j} (v_{i+1,j} - v_{i-1,j} - u_{i,j+1} + u_{i,j-1} + f_{i,j})^2 h_{i,j}^{-1},$$

- mass  $\sum_{i,j} h_{i,j}$ ,
- vorticity  $\sum_{i,j} \frac{1}{2\Delta x} \sum_{i,j} (v_{i+1,j} - v_{i-1,j} - u_{i,j+1} + u_{i,j-1} + f_{i,j})$ .

The AVF method [9] can be viewed as a generalization of the implicit midpoint rule which preserves quadratic Hamiltonians. It preserves higher order polynomial Hamiltonians, which includes the cubic Hamiltonian  $H$ . Quadratic Casimirs like mass and circulation are preserved exactly by AVF method. But higher-order polynomial Casimirs like the enstrophy (cubic) can not be preserved. Practical implementation of the AVF method requires the evaluation of the integral on the right hand side (7). Since the Hamiltonian  $\mathcal{H}$  and the discrete form of the Casimirs, potential enstrophy, mass and circulation are polynomial, they can be exactly integrated with a Gaussian quadrature rule of the appropriate degree. The AVF method is used with finite element discretization of the rotational SWE [1, 43] and for thermal SWE [44] in Poisson form. Although the fully implicit integrator gives the desired properties such as conservation of the energy, it is computationally expensive. Semi-implicit implementation of the AVF with a simplified Jacobian with a quasi-Newton solver is used for the thermal SWE in [44]. In [2] SWEs as a Poisson systems is discretized in space following [3] by the Arakawa-Lamb discretization [4] in space. It was shown that by using the time discretization with the non-structure preserving time integrators like the Adams-Basforth and Runge-Kutta methods, drifts occur in the energy and enstrophy [2]. A general approach to constructing schemes that conserve energy and potential enstrophy formulates the SWEs Nambu brackets [45], which is computationally expensive. Also it is not possible to preserve multiple integrals like the enstrophy at the same time [46] by geometric integrators like the AVF method. The SWE in a different Poisson form was discretized in space by compatible finite elements and solved in time using the AVF method [1, 43].

Semi-discretization of the SWE (5) leads to the following ODE system

$$\begin{aligned}\frac{du}{dt} &= -\mathbf{u} \circ (D_x \mathbf{u}) - v \circ (D_y \mathbf{u}) - g D_x \mathbf{h} + \mathbf{f} \circ \mathbf{v}, \\ \frac{dv}{dt} &= -\mathbf{u} \circ (D_x \mathbf{v}) - \mathbf{v} \circ (D_y \mathbf{v}) - g D_y \mathbf{h} - \mathbf{f} \circ \mathbf{u}, \\ \frac{dh}{dt} &= -D_x(\mathbf{h} \circ \mathbf{u}) - D_y(\mathbf{h} \circ \mathbf{v}).\end{aligned}$$

It can be rewritten using the Kronecker product as a quadratic ODE

$$\dot{\mathbf{z}} = F(\mathbf{z}) = Q_1(\mathbf{z}) + Q_2(\mathbf{z}) + L(\mathbf{z}), \quad (8)$$

$$Q_1(\mathbf{z}) = -AQ \left( \begin{pmatrix} \mathbf{u} \\ \mathbf{u} \\ \mathbf{u} \end{pmatrix} \otimes (B\mathbf{z}) \right), \quad Q_2(\mathbf{z}) = -CQ \left( \begin{pmatrix} \mathbf{v} \\ \mathbf{v} \\ \mathbf{v} \end{pmatrix} \otimes (D\mathbf{z}) \right), \quad L(\mathbf{z}) = \begin{pmatrix} \mathbf{f} \circ \mathbf{v} \\ -\mathbf{f} \circ \mathbf{u} \\ 0 \end{pmatrix} - g \begin{pmatrix} D_x \mathbf{h} \\ D_y \mathbf{h} \\ 0 \end{pmatrix},$$

where

$$A = \begin{pmatrix} I & I & D_x \end{pmatrix}, \quad B = \begin{pmatrix} D_x & D_x & I \end{pmatrix}, \quad C = \begin{pmatrix} I & I & D_y \end{pmatrix}, \quad D = \begin{pmatrix} D_y & D_y & I \end{pmatrix}.$$

with  $Q(x \otimes x) = x \circ x$ ,  $L \in \mathbb{R}^{3n \times 3n}$ ,  $Q \in \mathbb{R}^{3n \times (3n)^2}$ , and  $I$  is the identity matrix of size  $n \times n$ . The FOM (8) consists of a linear part  $L(\mathbf{z})$ , and quadratic parts  $Q_1(\mathbf{z}), Q_2(\mathbf{z})$ . For the quadratic ODE systems like (8), Kahan introduced an "unconventional" discretization [13] given by

$$\frac{\mathbf{z}^{n+1} - \mathbf{z}^n}{\Delta t} = Q_1(\mathbf{z}^n, \mathbf{z}^{n+1}) + Q_2(\mathbf{z}^n, \mathbf{z}^{n+1}) + \frac{1}{2}L(\mathbf{z}^n + \mathbf{z}^{n+1}).$$

The symmetric bilinear forms  $Q_1(\cdot, \cdot)$  and  $Q_2(\cdot, \cdot)$  are computed by the polarization of the quadratic vector fields  $Q_1(\cdot)$  and  $Q_2(\cdot)$  [47]

$$Q_1(\mathbf{z}^n, \mathbf{z}^{n+1}) = \frac{1}{2} (Q_1(\mathbf{z}^n + \mathbf{z}^{n+1}) - Q_1(\mathbf{z}^n) - Q_1(\mathbf{z}^{n+1})).$$

$Q_2(\cdot)$  is polarized in the same form. Kahan's method is second order and time-reversal and linearly implicit, i.e requires only one Newton iteration per time step [48]:

$$\left( I - \frac{\Delta t}{2} F'(\mathbf{z}^n) \right) \frac{\mathbf{z}^{n+1} - \mathbf{z}^n}{\Delta t} = F(\mathbf{z}^n), \quad (9)$$

where  $F'$  denotes the Jacobian of  $F$ .

A different polarization for polynomial Hamiltonians were introduced in [10] leading to linearly implicit discrete gradient methods. But this method is restricted to non-canonical Hamiltonian systems with constant Poisson matrix. Therefore it can not be applied to the rotational SWE (1) with state-dependent Poisson matrix. Recently in [49] a two-step version of Kahan's method is developed for non-canonical Hamiltonians with constant Poisson matrix that preserves Hamiltonian. But this method is not applicable to the SWE due to state-dependent Poisson matrix in (2).

#### 4. Reduced order model

In this section, we give the construction of two reduced order models for the SWE. The first one preserves the Hamiltonian for the SWE in Poisson form (1) using POD/DEIM. The second one preserves the linear-quadratic structure for the SWE in the  $f$ -plane representation (5) by applying tensorial POD.

##### 4.1. Hamiltonian preserving reduced order modelling with POD/DEIM

The semi-discretized SWE in Hamiltonian form (6) represents a nonlinear ODE of the form

$$\frac{d\mathbf{z}}{dt} = F(\mathbf{z}) = J(\mathbf{z})\bar{\nabla}H(\mathbf{z}), \quad (10)$$

where the state variable  $\mathbf{z} \in \mathbb{R}^{3n}$ . In reduced order modeling of fluid dynamics problems to avoid the fluctuations, the mean centered snapshots are collected at time instances  $t_i, i = 1, \dots, m$ , in the snapshot matrices  $S_u$ ,  $S_v$  and  $S_h$  [36, 50]

$$\begin{aligned} S_u &= (\mathbf{u}^1 - \bar{\mathbf{u}}, \mathbf{u}^2 - \bar{\mathbf{u}}, \dots, \mathbf{u}^m - \bar{\mathbf{u}}) \in \mathbb{R}^{n \times m} \\ S_v &= (\mathbf{v}^1 - \bar{\mathbf{v}}, \mathbf{v}^2 - \bar{\mathbf{v}}, \dots, \mathbf{v}^m - \bar{\mathbf{v}}) \in \mathbb{R}^{n \times m} \\ S_h &= (\mathbf{h}^1 - \bar{\mathbf{h}}, \mathbf{h}^2 - \bar{\mathbf{h}}, \dots, \mathbf{h}^m - \bar{\mathbf{h}}) \in \mathbb{R}^{n \times m}, \end{aligned}$$

where  $\mathbf{u}^i \approx \mathbf{u}(t_i)$ ,  $\mathbf{v}^i \approx \mathbf{v}(t_i)$ ,  $\mathbf{h}^i \approx \mathbf{h}(t_i)$ , and  $\bar{\mathbf{u}}$ ,  $\bar{\mathbf{v}}$  and  $\bar{\mathbf{h}}$  denote the mean of the snapshots

$$\bar{\mathbf{u}} = \frac{1}{m} \sum_{i=1}^m \mathbf{u}^i, \quad \bar{\mathbf{v}} = \frac{1}{m} \sum_{i=1}^m \mathbf{v}^i, \quad \bar{\mathbf{h}} = \frac{1}{m} \sum_{i=1}^m \mathbf{h}^i.$$

We have collected the velocity components  $\mathbf{u}$  and  $\mathbf{v}$ , and the height  $\mathbf{h}$  separately in snapshot matrices. The velocity components  $\mathbf{u}$  and  $\mathbf{v}$  are stacked in column vectors [50]

$$\begin{array}{c} \left( \begin{array}{ccc} \vdots & \dots & \vdots \\ \mathbf{u}_{1^k} & \ddots & \mathbf{u}_{n^k} \\ \vdots & \dots & \vdots \end{array} \right) \xrightarrow{\text{stack}} \left( \begin{array}{c} \mathbf{u}_{1^k} \\ \vdots \\ \mathbf{u}_{n^k} \end{array} \right) \in \mathbb{R}^{2n} \\ \xleftarrow{\text{unstack}} \left( \begin{array}{ccc} \vdots & \dots & \vdots \\ \mathbf{v}_{1^k} & \ddots & \mathbf{v}_{n^k} \\ \vdots & \dots & \vdots \end{array} \right) \left( \begin{array}{c} \mathbf{v}_{1^k} \\ \vdots \\ \mathbf{v}_{n^k} \end{array} \right) \end{array} \quad (11)$$

The POD basis functions are computed by applying the (thin) singular value decomposition (SVD)

$$S_u = V_u \Sigma_u W_u^T, \quad S_v = V_v \Sigma_v W_v^T, \quad S_h = V_h \Sigma_h W_h^T$$

to the snapshot matrices for the velocity components and the height component separately. The columns of the orthonormal matrices  $V_i \in \mathbb{R}^{n \times m}$  and  $W_i \in \mathbb{R}^{m \times m}$  are the left and right singular vectors of the snapshot matrix  $S_i$ , respectively,  $i = u, v, h$ . The diagonal matrix  $\Sigma_i = \text{diag}(\sigma_{i,1}, \sigma_{i,2}, \dots, \sigma_{i,m}) \in \mathbb{R}^{m \times m}$  contains the singular values of  $S_i$ . The singular vectors for the velocity components  $\mathbf{u}$  and  $\mathbf{v}$  are selected by unstacking (11). The r-POD basis matrix  $V_{i,r} \in \mathbb{R}^{n \times r}$  consists of the first  $r$  columns of  $V_i$ . The POD basis minimizes the following least squares error

$$\min_{V_{i,r} \in \mathbb{R}^{n \times r}} \|S_i - V_{i,r} V_{i,r}^T\|_F^2 = \sum_{k=r+1}^n \sigma_{i,k}^2.$$

Thus the error in the snapshot representation is given by the sum of the squares of the singular values corresponding to those left singular vectors which are not included in the POD basis. The singular values provide quantitative guidance for choosing the size of the POD basis, that accurately represent the given snapshot data. Usually the following relative "cumulative energy" criteria is used

$$\frac{\sum_{k=1}^r \sigma_k^2}{\sum_{k=1}^m \sigma_k^2} > \kappa, \quad (12)$$

where  $\kappa$  is a user-specified tolerance, typically taken to be 99% or greater. For  $\bar{\mathbf{z}} = (\bar{\mathbf{u}}^T, \bar{\mathbf{v}}^T, \bar{\mathbf{h}}^T)^T$ , the state  $\mathbf{z} = (\mathbf{u}^T, \mathbf{v}^T, \mathbf{h}^T)^T$  is then approximated in the POD subspace spanned by the first  $r$  POD basis as

$$\mathbf{z} \approx \tilde{\mathbf{z}} = \bar{\mathbf{z}} + V_r \mathbf{z}_r, \quad V_r = \begin{pmatrix} V_{u,r} & & \\ & V_{v,r} & \\ & & V_{h,r} \end{pmatrix} \in \mathbb{R}^{3n \times 3r}, \quad (13)$$

where  $\mathbf{z}_r$  is the  $3r$ -dimensional reduced state. By substituting (13) into (10) and applying the Galerkin projection, the following  $3r$ -dimensional mean centered POD reduced model is obtained

$$\frac{d\mathbf{z}_r(t)}{dt} = V_r^T F(\tilde{\mathbf{z}}(t)), \quad \mathbf{z}_r(0) = V_r^T (\mathbf{z}(0) - \bar{\mathbf{z}}). \quad (14)$$

The ROM (14) with the discrete energy  $H(\tilde{\mathbf{z}})$ , does not necessarily satisfy the invariance of the discrete energy for all time. But the updated ROM

$$\frac{d\mathbf{z}_r}{dt} = \tilde{J}_r(\tilde{\mathbf{z}}) \widetilde{\nabla H}_r(\tilde{\mathbf{z}}) \quad (15)$$

with the updated reduced skew-symmetric matrix  $\tilde{J}_r(\tilde{\mathbf{z}}) = V_r^T J(\tilde{\mathbf{z}}) V_r$  and the updated reduced gradient of the Hamiltonian  $\widetilde{\nabla H}_r(\tilde{\mathbf{z}}) = V_r^T \mathbf{z} \nabla H(\tilde{\mathbf{z}})$ , preserves the energy for all time [31, 32].

The cost of evaluating  $F(\cdot)$  scales not only with the dimension  $r$  of the ROM, also with the dimension the FOM,  $n$ . The computational cost is reduced by sampling the nonlinearity  $F(\cdot)$  a subset of the elements of  $V_r$  and interpolating, known as hyper-reduction techniques. Several hyper-reduction methods are developed to reduce the computations cost of evaluating the reduced nonlinear terms, empirical interpolation (EIM) [15], discrete empirical interpolation (DEIM) [16], QDEIM [51], missing point estimation [17], best points interpolation [19], gappy POD [20]. We use the DEIM, which is one the most frequently used hyper-reduction method. Rigorous error and stability analysis are in general not amenable for sampling procedures used in hyper-reduction methods.

We apply the DEIM to the ODE form (10) of SWE together with the AVF time integrator, and the ROM (15) is also integrated by AVF. Thus, in order to proceed with the DEIM, the AVF applied nonlinear snapshots are collected on time intervals  $[t_n, t_{n+1}]$ ,  $n = 1, \dots, m-1$ , in the snapshot matrices  $G_i$ ,  $i = 1, 2, 3$ ,

$$G_i = \left( \int_0^1 \overline{\nabla H}_i(\mathbf{z}_\xi^2) d\xi, \int_0^1 \overline{\nabla H}_i(\mathbf{z}_\xi^3) d\xi, \dots, \int_0^1 \overline{\nabla H}_i(\mathbf{z}_\xi^m) d\xi \right) \in \mathbb{R}^{3n \times (m-1)},$$

where we set  $\mathbf{z}_\xi^n := \xi(\mathbf{z}^n - \mathbf{z}^{n-1}) + \mathbf{z}^{n-1}$ ,  $n = 2, \dots, m$ , and each  $\nabla H_i$  corresponds to the nonlinearity in one of the three equations in the semi-discrete system of SWE. Then, we can approximate each  $\int_0^1 \nabla H_i(\mathbf{z}_\xi^n) d\xi$  in the column space of the snapshot matrices  $G_i$ . We first apply POD to the snapshot matrices  $G_i$  and find the matrices  $V_i^d \in \mathbb{R}^{n \times k}$  whose columns are the basis functions spanning the column space of the snapshot matrices  $G_i$ . Then, we apply the DEIM algorithm [16] to find projection matrices  $P_i \in \mathbb{R}^{n \times k}$  so that we have

$$\int_0^1 \nabla H_i(\mathbf{z}_\xi^n) d\xi \approx \mathcal{V}_i^d P_i^T \int_0^1 \nabla H_i(\mathbf{z}_\xi^n) d\xi = \mathcal{V}_i^d \int_0^1 P_i^T \nabla H_i(\mathbf{z}_\xi^n) d\xi,$$

where  $\mathcal{V}_i^d = V_i^d (P_i^T V_i^d)^{-1} \in \mathbb{R}^{n \times k}$  is precomputed in the offline stage, and by the term  $P_i^T \nabla H_i(\mathbf{z}_\xi^n) \in \mathbb{R}^k$ , we need to compute only  $k \ll n$  entry of the nonlinear vector. In addition, the computational complexity for the Jacobian matrix reduces from  $\mathcal{O}(n^2)$  to  $\mathcal{O}(kn)$ . By using DEIM approximation, the full discrete ROM with POD/DEIM reads as

$$\mathbf{z}_r^{n+1} = \mathbf{z}_r^n + \Delta t \tilde{J}_r V_r^T \begin{pmatrix} \mathcal{V}_1^d & & \\ & \mathcal{V}_2^d & \\ & & \mathcal{V}_3^d \end{pmatrix} \begin{pmatrix} \int_0^1 P_1^T \nabla H_1(\mathbf{z}_\xi^{n+1}) d\xi \\ \int_0^1 P_2^T \nabla H_2(\mathbf{z}_\xi^{n+1}) d\xi \\ \int_0^1 P_3^T \nabla H_3(\mathbf{z}_\xi^{n+1}) d\xi \end{pmatrix}.$$

In case of the selection of the number  $k$  of DEIM basis functions, the "cumulative energy" criteria (12) is used, as well. But, because of the nature of the nonlinearity, snapshot matrices are more sensitive and larger number of modes are needed for well reflection, we take  $\kappa$  now 99.99% or greater.

#### 4.2. Tensorial POD

For PDEs and ODEs with polynomial nonlinearities, ROMs do not require approximating the nonlinear function  $F(\cdot)$  through sampling, the reduced order operators can be precomputed in the offline stage. This is beneficial because the offline-online computation is separated in contrast to the hyper-reduction methods. In the past, for the Navier-Stokes [52, 53] equation, the quadratic polynomial forms of the FOMs are exploited by constructing reduced models. For polynomial nonlinearities the ROMs preserve the linear-quadratic structure.

The mean-centered ROM for (9) takes the form

$$\left( I - \frac{\Delta t}{2} F'(\tilde{\mathbf{z}}^n) V_r \right) \frac{\mathbf{z}_r^{n+1} - \mathbf{z}_r^n}{\Delta t} = V_r^T F(\tilde{\mathbf{z}}^n).$$

where

$$V_r = \begin{pmatrix} V_u & 0 & 0 \\ 0 & V_v & 0 \\ 0 & 0 & V_h \end{pmatrix},$$

and  $V_u, V_v, V_h \in \mathbb{R}^{n \times r}$  are the matrices containing the POD modes for the state vectors  $\mathbf{u}, \mathbf{v}, \mathbf{h}$ , respectively. Substituting (13) into (8) and applying Galerkin

approximation, we obtain the following linear-quadratic POD-ROM

$$\frac{d\mathbf{z}_r}{dt} = F_r(\tilde{\mathbf{z}}) = L_r\tilde{\mathbf{z}} + Q_r(\tilde{\mathbf{z}} \otimes \tilde{\mathbf{z}}), \quad (16)$$

with the precomputed reduced order operators

$$L_r = V_r^T L V_r, \quad Q_r = V_r^T Q (V_r \otimes V_r).$$

This avoids the approximation of the nonlinear terms by hyper-reduction and allows separation of offline and online computation of FOM and ROM.

By introducing the reduced order solutions and operators, the linear-quadratic reduced equation (16) becomes

$$V_r^T F(\bar{\mathbf{z}} + V_r(\mathbf{z}_r)) = V_r^T (Q_1(\bar{\mathbf{z}} + V_r\mathbf{z}_r) + Q_2(\bar{\mathbf{z}} + V_r\mathbf{z}_r)) + V_r^T L V_r(\bar{\mathbf{z}} + V_r\mathbf{z}_r).$$

We can compute  $V_r^T Q_1(\bar{\mathbf{z}} + V_r\mathbf{z}_r)$  as follows

$$\begin{aligned} V_r^T Q_1(\bar{\mathbf{z}} + V_r\mathbf{z}_r) &= -V_r^T A Q \left( \begin{pmatrix} \bar{\mathbf{u}} + V_u \mathbf{u}_r \\ \bar{\mathbf{u}} + V_u \mathbf{u}_r \\ \bar{\mathbf{u}} + V_u \mathbf{u}_r \end{pmatrix} \otimes (B\tilde{\mathbf{z}}) \right), \\ &= -V_r^T A Q \left( \begin{pmatrix} \bar{\mathbf{u}} \\ \bar{\mathbf{u}} \\ \bar{\mathbf{u}} \end{pmatrix} \otimes (B\bar{\mathbf{z}}) + \begin{pmatrix} \bar{\mathbf{u}} \\ \bar{\mathbf{u}} \\ \bar{\mathbf{u}} \end{pmatrix} \otimes (BV_r\mathbf{z}_r) \right) \quad (17) \\ &\quad - V_r^T A Q \left( \begin{pmatrix} V_u \mathbf{u}_r \\ V_u \mathbf{u}_r \\ V_u \mathbf{u}_r \end{pmatrix} \otimes (B\bar{\mathbf{z}}) + \begin{pmatrix} V_u \mathbf{u}_r \\ V_u \mathbf{u}_r \\ V_u \mathbf{u}_r \end{pmatrix} \otimes (BV_r\mathbf{z}_r) \right) \end{aligned}$$

The nonlinear term above is computed by the Kronecker product as follows

$$\begin{aligned} -V_r^T A Q \left( \begin{pmatrix} V_u \mathbf{u}_r \\ V_u \mathbf{u}_r \\ V_u \mathbf{u}_r \end{pmatrix} \otimes (BV_r\mathbf{z}_r) \right) &= -V_r^T A Q (\bar{V}_u \otimes (BV_r)) \left( \begin{pmatrix} \mathbf{u}_r \\ \mathbf{u}_r \\ \mathbf{u}_r \end{pmatrix} \otimes (\mathbf{z}_r) \right) \\ &= Q_r \left( \begin{pmatrix} \mathbf{u}_r \\ \mathbf{u}_r \\ \mathbf{u}_r \end{pmatrix} \otimes (\mathbf{z}_r) \right) \end{aligned}$$

where  $Q_r = -V_r^T A Q (\bar{V}_u \otimes (BV_r))$  and

$$\bar{V}_u = \begin{pmatrix} V_u & & \\ & V_u & \\ & & V_u \end{pmatrix}.$$

The other quadratic term  $Q_2$  can be computed in the same way. In [37, 36] the semi-discrete form of SWE in the  $\beta$ -plane leads also to a linear quadratic ODE system like (8). They construct the reduced tensor  $\mathcal{Q}_r \in \mathbb{R}^{3r \times 3r \times 3r}$  as follows

$$\mathcal{Q}_r = \left[ \mathcal{Q}_r^{(i,j,k)} \right]_{i,j,k=1,\dots,3r}, \quad \mathcal{Q}_r^{(i,j,k)} = \sum_{l=1}^{3n} W(l,i) G(l,j) \bar{V}_u(l,k),$$

where  $G = BV \in \mathbb{R}^{3n \times 3r}$  and  $W = -A^T V_r$ . Then, the reduced matrix  $Q_r$  can be constructed by the mode-1 unfolding of the reduced tensor  $\mathcal{Q}_r \in \mathbb{R}^{3r \times 3r \times 3r}$ . It was shown that the tensorial POD (TPOD) has online complexity  $\mathcal{O}(r^3)$  and DEIM has  $\mathcal{O}(rk)$ , where  $k$  is the number of interpolation points. In [37, 36] TPOD was computed using Frobenious dot products, therefore the TPOD was slower than the DEIM. Below we give two new approaches which reduces the computational cost of the TPOD significantly.

The special structure of the matrix  $Q$  which represents the Hessian of right-hand side of (8) will be exploited in computation of TPOD [21]. The matrix  $Q$  is sparse due to the local structure of common discretizations like finite differences, finite elements for homogeneous polynomial nonlinearities. For the SWE with quadratic nonlinear terms, the cross terms  $z_i \cdot z_j$  vanish for  $|i - j| > 3$  in the semi-discretized ODE (8). Therefore the number of nonzero columns of  $Q$  are  $2n$  only. The matrix  $Q$  is an unfolding of the 3-tensor  $\mathcal{Q} \in \mathbb{R}^{3n \times 3n \times 3n}$ . Reshaping the tensor  $\mathcal{Q}$  into a matrix is called matricization, because working with matrices instead of tensors is beneficial. A common matricization of  $\mathcal{Q}$  is the so called  $\mu$ -mode matricization  $Q^{(\mu)}$  [21]. For example  $Q^{(1)}$  is called mode 1-matricization of  $\mathcal{Q}$ . For mode-2 and mode-3 matricizations, we refer to [21]. Using the matricization of the tensors, tensor matrix multiplication is equivalently determined by matrix-matrix products. The main computational burden in TPOD is computation of  $V_r \otimes V_r$ , which has complexity of order  $\mathcal{O}((nr)^2)$  for quadratic nonlinearities. In [21] an algorithm is developed to construct the reduced Hessian  $Q_r \in \mathbb{R}^{r \times r \times r}$  which avoids the computation of  $V_r \otimes V_r$ .

Below we give the TPOD algorithm in [21] for the quadratic nonlinear term  $Q_1$ . In (17) the computation of  $Q_r = -V_r^T A Q (\bar{V}_u \otimes (BV_r)) \in \mathbb{R}^{(3r)^2 \times 3r}$  will be inefficient due to the dense structure of the reduced matrix  $V_u$ , i.e.  $\bar{V}_u \otimes (BV_r) \in \mathbb{R}^{(3nr)^2}$ . Using the  $\mu$ -mode (matrix) product the POD modes can be efficiently computed as following [21]:

- Compute  $\mathcal{Y}^{3r \times 3n \times 3n}$  by  $Y^{(1)} = -V_r^T A Q$ ,
- Compute  $\mathcal{Z}^{3r \times 3r \times 3n}$  by  $Z^{(2)} = V_r^T B^T Y^{(2)}$ ,
- Compute  $\mathcal{Q}_r^{3r \times 3r \times 3r}$  by  $Q_r^{(3)} = \bar{V}_u^T Z^{(3)}$ .

Because the matrix  $Q$  is sparse and has  $\mathcal{O}(n)$  nonzero columns,  $V_r^T A Q$  will not result in a dense matrix, i.e. it has not the complexity of  $\mathcal{O}(rn^2)$ . This enables the efficient computation of the POD modes for large quadratic systems. At each step the tensor multiplication is performed by means of matricization.

The reduced linear-quadratic is solved by Kahan's method with the Jacobian evaluated using the following tensorial form

$$Q_r \left( \hat{I} \otimes \mathbf{z}_r^n + \begin{pmatrix} \mathbf{z}_r^n \\ \mathbf{z}_r^n \\ \mathbf{z}_r^n \end{pmatrix} \otimes \tilde{I} \right),$$

where

$$\tilde{I} = \begin{pmatrix} I_r & & \\ & I_r & \\ & & I_r \end{pmatrix} \in \mathbb{R}^{3r \times 3r}, \quad \hat{I} = \begin{pmatrix} I_r & \mathbf{0} & \mathbf{0} \\ I_r & \mathbf{0} & \mathbf{0} \\ I_r & \mathbf{0} & \mathbf{0} \end{pmatrix} \in \mathbb{R}^{3r \times 3r}.$$

Recently a new TPOD approach was developed for a more efficient computation of the reduced matrix  $Q_r$  using the particular structure of Kronecker product [22, 23]. Although the  $\mu$ -mode (matrix) product decreases the complexity of evaluating the reduced matrix  $Q_r$ , still the matrix  $Q$  has to be build for each different polynomial nonlinearities. A more compact form of the evaluation of the reduced matrix  $Q_r$  is given in MATLAB notation as follows [22, 23]:

$$\begin{aligned} Q_r &= -V^\top A Q (\bar{V}_u \otimes BV) \\ &= -V^\top A Q (\bar{V}_u \otimes G) \\ &= -V^\top A \begin{pmatrix} \bar{V}_u(1,:) \otimes G(1,:) \\ \vdots \\ \bar{V}_u(3n,:) \otimes G(3n,:) \end{pmatrix}, \end{aligned} \quad (18)$$

where  $G = BV \in \mathbb{R}^{3n \times 3r}$  and the complexity of this operation is  $\mathcal{O}(3n(3r)^3)$ . Thus, the reduced matrix  $Q_r$  can be constructed without explicitly defining the matrix  $Q$ . The transpose of the Kronecker products of any given two vectors  $\mathbf{a}$  and  $\mathbf{b}$  can be represented as follows

$$\begin{aligned} (\text{vec}(\mathbf{b}\mathbf{a}^\top))^\top &= (\mathbf{a} \otimes \mathbf{b})^\top \\ &= \mathbf{a}^\top \otimes \mathbf{b}^\top, \end{aligned} \quad (19)$$

where  $\text{vec}(\cdot)$  denotes vectorization of a matrix. Using (19), the matrix  $N = Q(V_u \otimes G) \in \mathbb{R}^{3n \times 9r^2}$  in (18) can be constructed as follows  $N(i,:) = (\text{vec}(G(i,:)^\top V_u(i,:)))^\top$ ,  $i \in \{1, 2, \dots, 3n\}$ . In [22, 23] the so called CUR [54], an pseudo-skeletal matrix approximation is used to increase computational efficiency. Here we make use of "MULTIPROD" [55] to reduce the complexity of the reduced nonlinear terms. MULTIPROD use virtual array expansion to perform multiple matrix products. Now, if we reshape the matrix  $V_u$  as  $V_u \in \mathbb{R}^{3n \times 1 \times 3r}$  and compute MULTIPROD of  $G$  and  $V_u$  in 2 and 3 dimensions. MULTIPROD assigns virtually a singleton to the third dimension of  $G$  which  $\mathcal{N} = \text{MULTIPROD}(G, V_u) \in \mathbb{R}^{3n \times 3r \times 3r}$ . Thus, we can represent (18) as  $Q_r = -V^\top A \mathcal{N}^{(1)}$ .

## 5. Numerical results

We consider the SWE on the spatial domain  $\Omega = [0, 1]^2$ , with data  $g = 1, f = 0$ , and with the initial conditions

$$\begin{aligned} h(x, y, 0) &= 1 + (1/2) \exp[-25(x - 1/2)^2 - 25(y - 1/2)^2], \\ u(x, y, 0) &= -\sin(\pi x) \sin(2\pi y)/2\pi, \\ v(x, y, 0) &= \sin(2\pi x) \sin(\pi y)/2\pi. \end{aligned}$$

Periodic boundary conditions [56] are prescribed. The final time is set to  $T = 50$ , and spatial and temporal mesh sizes are taken as  $\Delta x = 0.01$  and  $\Delta t = 4\Delta x$ , respectively. All simulations are performed on a Windows 10 machine with Intel Core i7, 2.5 GHz and 8 GB using MATLAB R2014. CPU time is measured in seconds.

The singular values of the snapshot matrices for both methods are plotted in the semi-logarithmic scale in Figure 1, with the index of singular values on the horizontal axis. The singular values decay for both methods slowly, which is the characteristic of the problems with wave phenomena in fluid dynamics.

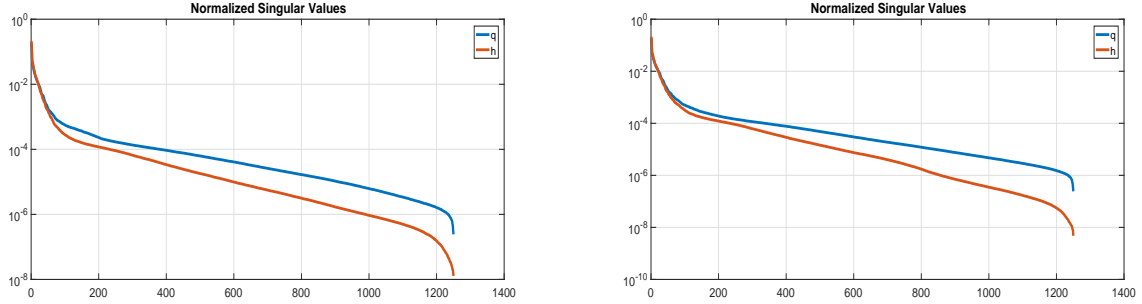


Figure 1: Singular values: (left) AVF, (right) Kahan.

The  $L_2 - L_2$  errors in Figure 2 for the state variables with respect to the number of POD modes decrease similarly for both methods, in which the slow decay of the singular values in Figure 1 is reflected to slow decreasing behavior of the ROM errors. The number of POD modes in further computations are selected as 30, according to the relative energy criteria (12) with  $\kappa = 99.99\%$ . Using the same criteria the number of DEIM interpolation points are selected as 90.

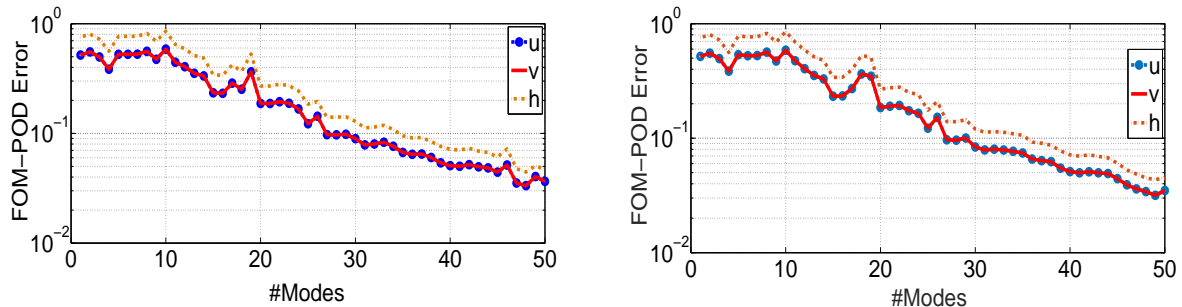


Figure 2:  $L_2(L_2)$  Error vs. number of POD modes: (left) Kahan, (right) AVF.

The FOM solutions for the state variables for both methods are similar in Figure 3. The FOM solutions are captured well by the POD/DEIM with the AVF method, and TPOD with the Kahan's method in Figure 4. The errors

for approximate solutions and conserved quantities are the same by POD and TPOD.

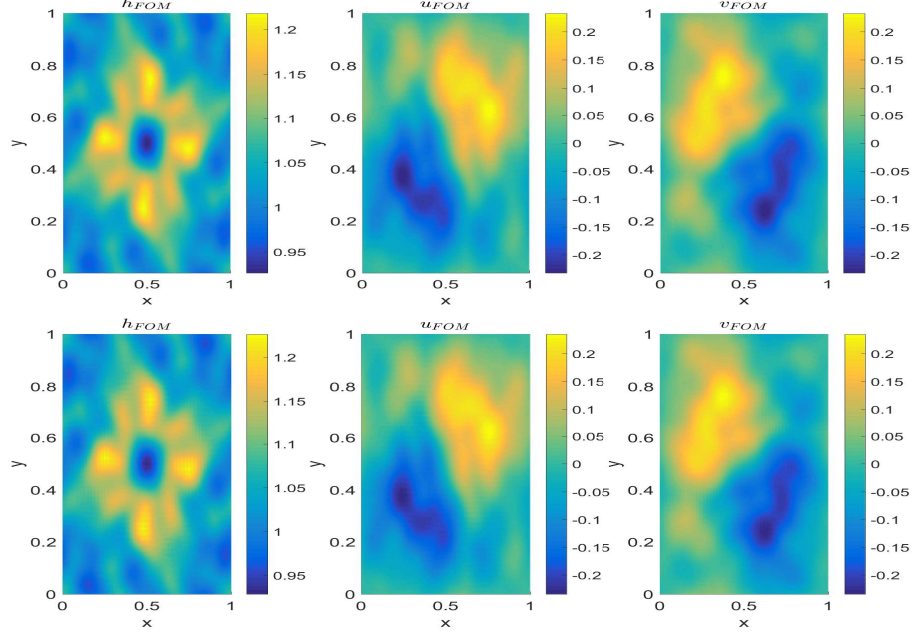


Figure 3: FOM solution at final time  $T = 50$ : (top) AVF, (bottom) Kahan.

The energy, enstrophy and vorticity are well preserved in Figures 5-7. Because the vorticity is a quadratic Casimir, it shows no drift over time, Figure 7. The energy and enstrophy have cubic terms, therefore they show some drifts (for the POD in the AVF method), but the ROM solutions with POD/DEIM and TPOD have bounded oscillations over the time, i.e. they are preserved with some accuracy. The mass is preserved up to machine precision since it is a linear conserved quantity, and it was not shown.

To illustrate the FOM-ROM state errors, we use time averaged relative  $L_2$ -error defined by

$$\frac{1}{m} \sum_{i=1}^m \frac{\|\mathbf{z}(:, t_i) - \tilde{\mathbf{z}}(:, t_i)\|_2}{\|\mathbf{z}(:, t_i)\|_2},$$

and for conservation of the energy, enstrophy, and vorticity, we use the following time-averaged relative FOM-ROM error

$$\frac{1}{m} \sum_{i=1}^m |E(t_i) - E(t_0)|.$$

Table 1 shows that the FOM-ROM state errors are very close for the POD/DEIM and TPOD. The invariants are more accurately preserved by the POD using

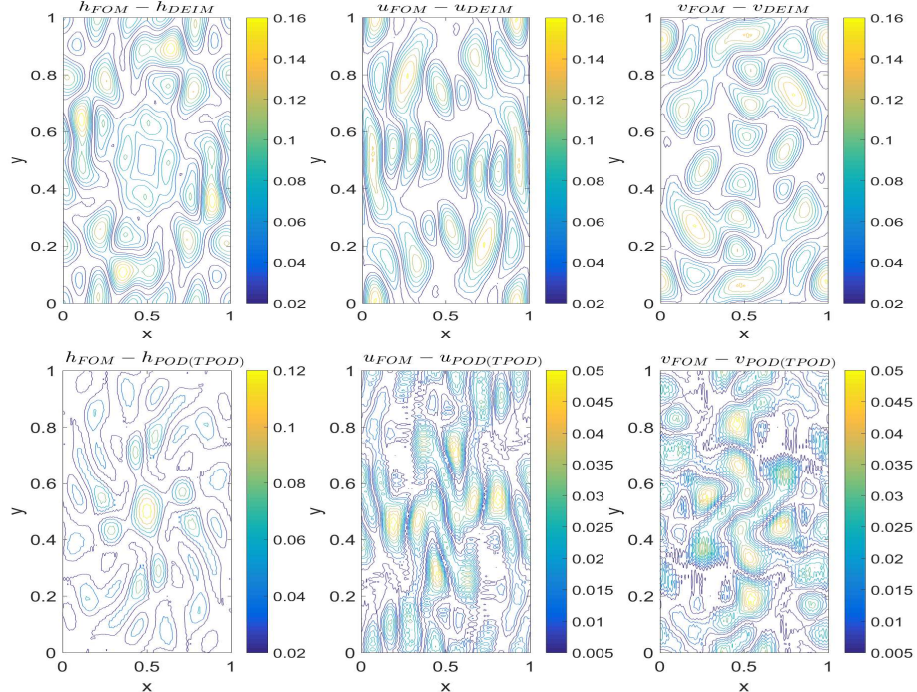


Figure 4: FOM-ROM errors: (top) POD/DEIM and (bottom) TPOD at the final time  $T = 50$ .

AVF method, and by the TPOD with Kahan's method, Table 2. The energy and vorticity errors for POD/DEIM are larger than POD and TPOD. This was also pointed out in [25] that for some problems large number of DEIM interpolation points are required to achieve accurate solutions, which increases the computational cost of the ROMs in online computation as in Tables 3 and 4.

The CPU times in Tables 3-4 show the computational efficiency of the TPOD over POD/DEIM due to the separation of offline-online computation, and by preserving the quadratic structure of semi-discretized SWE by TPOD. The computational efficiency is further increased by exploiting the sparse matrix structure of the discretized SWE using MULTIPROD in the TPOD algorithm of [22, 23] over [21] as shown in Figure 8. A similar behavior was observed for both TPOD algorithms in [22] using CUR approximation [54].

Table 1: Time averaged relative FOM-ROM error for 30 POD/TPOD modes and for 90 DEIM modes.

		<b>u</b>	<b>v</b>	<b>h</b>
AVF	POD	1.192e-01	1.192e-01	1.473e-02
	DEIM	2.874e-01	2.874e-01	3.478e-02
Kahan	POD-TPOD	1.265e-01	1.265e-01	1.567e-02

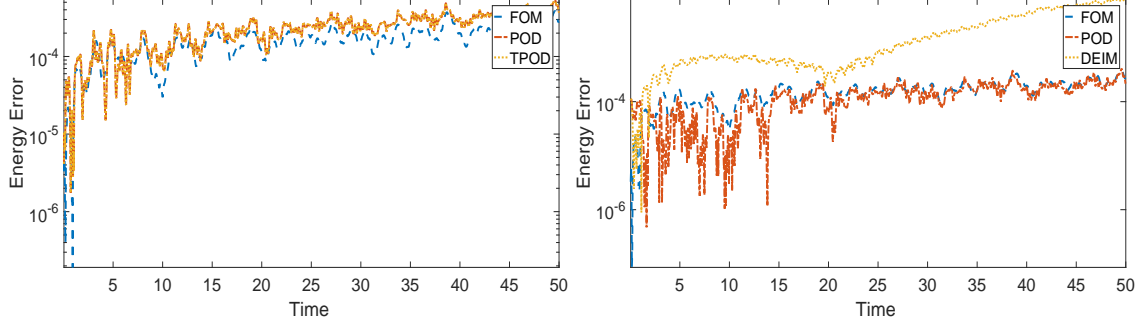


Figure 5: Energy: (left) Kahan, (right) AVF.

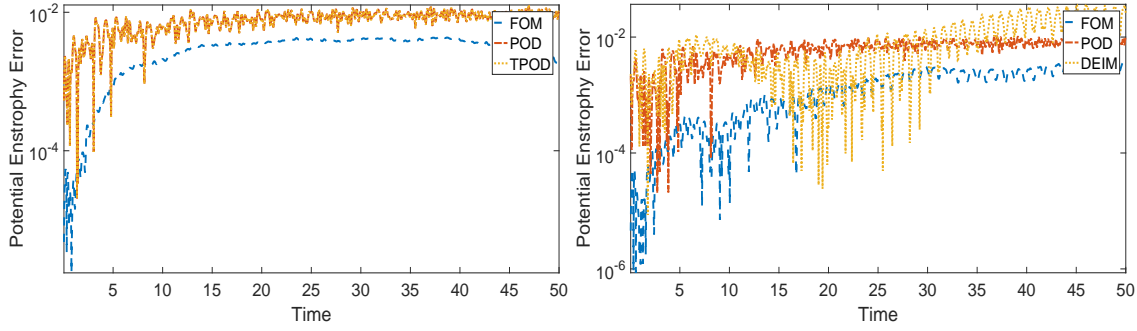


Figure 6: Enstrophy: (left) Kahan, (right) AVF.

Table 2: Absolute FOM-ROM errors for 30 POD/TPOD modes and for 90 DEIM modes.

		Energy	Enstrophy	Vorticity
AVF	POD	3.768e-05	7.871e-03	2.123e-05
	POD/DEIM	1.968e-03	5.137e-03	1.042e-03
Kahan	POD-TPOD	2.901e-05	3.108e-03	3.454e-05

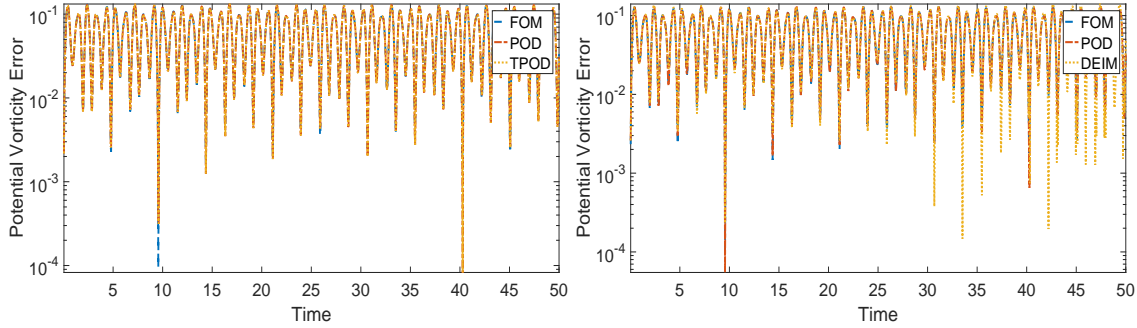


Figure 7: Vorticity: (left) Kahan, (right) AVF.

Table 3: CPU time in seconds for 30 POD basis and for 90 DEIM modes.

AVF			Kahan		
	FOM	529.80		FOM	788.89
POD	basis computation	33.46	POD	basis computation	31.02
	online computation	291.69		online computation	289.01
	total	325.15		total	321.03
DEIM	basis computation	33.89	TPOD	tensor computation [21]([22])	20.78 (9.43)
	online computation	24.10		online computation	6.42
	total	57.99		total [21]([22])	27.20 (15.89)

Table 4: Speed-up factors.

AVF		Kahan		
POD	DEIM	POD	TPOD [21]([22])	
1.63	9.13	2.45	29.00 (49.64)	

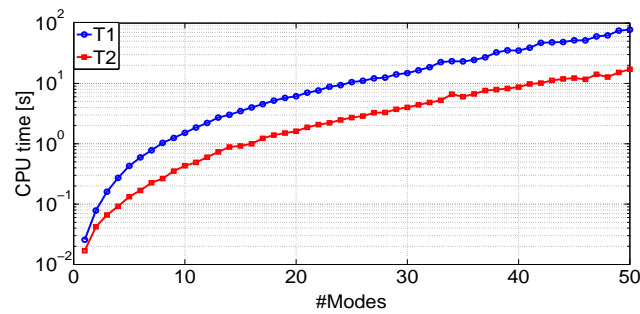


Figure 8: Tensor calculations for 10.000 grid points: T1 [21], T2 [22].

## 6. Conclusions

Using Hamiltonian and quadratic form of the SWE, we have constructed ROMs which preserve both structure. Numerical results showed that the conserved quantities are well preserved in the reduced order models, which are important for the stable solutions in long term integration. Because the singular values decay slowly, relatively more POD and DEIM modes required. This is a characteristic for problems with wave type solutions in fluid dynamics. Both POD/DEIM and TPOD produced accurate solutions, whereas TPOD are computationally more efficient. As the next task we will build ROMs for the single and multi-layer SWE with complete Coriolis force [2] which are more complex then the SWE with constant Coriolis force, and investigate the preservation of the conserved quantities in long term integration by the AVF method and Kahan's method.

**Acknowledgements** This work was supported by 100/2000 Ph.D. Scholarship Program of Turkish Higher Education Council.

## References

- [1] Bauer W., Cotter C.J.. Energy-enstrophy conserving compatible finite element schemes for the rotating shallow water equations with slip boundary conditions. *Journal of Computational Physics*. 2018;373:171 - 187.
- [2] Stewart Andrew L., Dellar Paul J.. An energy and potential enstrophy conserving numerical scheme for the multi-layer shallow water equations with complete Coriolis force. *Journal of Computational Physics*. 2016;313:99 - 120.
- [3] Salmon Rick. Poisson-bracket approach to the construction of energy- and potential-enstrophy-conserving algorithms for the shallow-water equations. *Journal of the Atmospheric Sciences*. 2004;61(16):2016-2036.
- [4] Arakawa Akio, Lamb Vivian R.. A potential enstrophy and energy conserving scheme for the shallow water equations. *Monthly Weather Review*. 1981;109(1):18-36.
- [5] Dellar Paul J., Salmon Rick. Shallow water equations with a complete Coriolis force and topography. *Physics of Fluids*. 2005;17(10):106601.
- [6] Hairer Ernst, Lubich Christian, Wanner Gerhard. *Geometric numerical integration: Structure-preserving algorithms for ordinary differential equations*. Springer Series in Computational MathematicsSpringer, Heidelberg; 2010.
- [7] Leimkuhler Benedict, Reich Sebastian. *Simulating Hamiltonian Dynamics*. Cambridge Monographs on Applied and Computational MathematicsCambridge University Press; 2005.

- [8] Celledoni, E. and Grimm, V. and McLachlan, R. I. and McLaren, D. I. and O’Neale, D. J. and Owren, B. and Quispel, G. R. W. . Preserving energy resp. dissipation in numerical PDEs using the ”Average Vector Field” method.. *J. Comput. Physics.* 2012;231:6770-6789.
- [9] Cohen David, Hairer Ernst. Linear energy-preserving integrators for Poisson systems. *BIT Numerical Mathematics.* 2011;51(1):91–101.
- [10] Dahlby M., Owren B.. A general framework for deriving integral preserving numerical methods for PDEs. *SIAM Journal on Scientific Computing.* 2011;33(5):2318-2340.
- [11] McLachlan Robert I., Quispel G. R. W., Robidoux Nicolas. Geometric integration using discrete gradients. *Philosophical Transactions of the Royal Society of London A: Mathematical, Physical and Engineering Sciences.* 1999;357(1754):1021–1045.
- [12] Quispel G.R.W., Capel H.W.. Solving ODEs numerically while preserving a first integral. *Physics Letters A.* 1996;218(3):223 - 228.
- [13] Kahan W.. *Unconventional Numerical Methods for Trajectory Calculations.* : Computer Science Division and Department of Mathematics, University of California, Berkeley; 1993. Unpublished lecture notes.
- [14] Celledoni Elena, McLachlan Robert I, Owren Brynjulf, Quispel G R W. Geometric properties of Kahan’s method. *Journal of Physics A: Mathematical and Theoretical.* 2013;46(2):025201.
- [15] Barrault Maxime, Maday Yvon, Nguyen Ngoc Cuong, Patera Anthony T.. An empirical interpolation method: application to efficient reduced-basis discretization of partial differential equations. *Comptes Rendus Mathematique.* 2004;339(9):667–672.
- [16] Chaturantabut Saifon, Sorensen Danny C.. Nonlinear model reduction via discrete empirical interpolation. *SIAM Journal on Scientific Computing.* 2010;32(5):2737–2764.
- [17] Astrid P., Weiland S., Willcox K., Backx T.. Missing point estimation in models described by proper orthogonal decomposition. *IEEE Transactions on Automatic Control.* 2008;53(10):2237-2251.
- [18] Zimmermann R., Willcox K.. An accelerated greedy missing point estimation procedure. *SIAM Journal on Scientific Computing.* 2016;38(5):A2827-A285.
- [19] Nguyen N. C., Patera A. T., Peraire J.. A ”best points” interpolation method for efficient approximation of parametrized functions. *International Journal for Numerical Methods in Engineering.* 2008;73(4):521-543.

- [20] Carlberg Kevin, Farhat Charbel, Cortial Julien, Amsallem David. The GNAT method for nonlinear model reduction: effective implementation and application to computational fluid dynamics and turbulent flows. *Journal of Computational Physics*. 2013;242:623 - 647.
- [21] Benner P., Breiten T.. Two-sided projection methods for nonlinear model order reduction. *SIAM Journal on Scientific Computing*. 2015;37(2):B239-B260.
- [22] Benner P., Goyal P., Gugercin S..  $\mathcal{H}_2$ -quasi-optimal model order reduction for quadratic-bilinear control systems. *SIAM Journal on Matrix Analysis and Applications*. 2018;39(2):983-1032.
- [23] Benner Peter, Goyal Pawan. Interpolation-based model order reduction for polynomial parametric systems. *arXiv e-prints*. 2019;.
- [24] Gu C.. QLMOR: a projection-based nonlinear model order reduction approach using quadratic-linear representation of nonlinear systems. *IEEE Transactions on Computer-Aided Design of Integrated Circuits and Systems*. 2011;30(9):1307-1320.
- [25] Kramer Boris, Willcox Karen E.. Nonlinear model order reduction via lifting transformations and proper orthogonal decomposition. *AIAA Journal*. 0;0(0):1-11.
- [26] Lall Sanjay, Krysl Petr, Marsden Jerrold E.. Structure-preserving model reduction for mechanical systems. *Phys. D*. 2003;184(1-4):304–318.
- [27] Carlberg Kevin, Tuminaro Ray, Boggs Paul. Preserving Lagrangian structure in nonlinear model reduction with application to structural dynamics. *SIAM J. Sci. Comput.*. 2015;37(2):B153–B184.
- [28] Chaturantabut S., Beattie C., Gugercin S.. Structure-preserving model reduction for nonlinear port-Hamiltonian systems. *SIAM Journal on Scientific Computing*. 2016;38(5):B837-B865.
- [29] Afkham Babak Maboudi, Hesthaven Jan S.. Structure preserving model reduction of parametric Hamiltonian systems. *SIAM Journal on Scientific Computing*. 2017;39(6):A2616-A2644.
- [30] Peng Liqian, Mohseni Kamran. Symplectic model reduction of Hamiltonian systems. *SIAM Journal on Scientific Computing*. 2016;38(1):A1-A27.
- [31] Gong Yuezheng, Wang Qi, Wang Zhu. Structure-preserving Galerkin POD reduced-order modeling of Hamiltonian systems. *Computer Methods in Applied Mechanics and Engineering*. 2017;315:780 - 798.
- [32] Karasözen Bülent, Uzunca Murat. Energy preserving model order reduction of the nonlinear Schrödinger equation. *Advances in Computational Mathematics*. 2018;44(6):1769–1796.

- [33] Lozovskiy Alexander, Farthing Matthew, Kees Chris, Gildin Eduardo. POD-based model reduction for stabilized finite element approximations of shallow water flows. *Journal of Computational and Applied Mathematics*. 2016;302:50 - 70.
- [34] Lozovskiy Alexander, Farthing Matthew, Kees Chris. Evaluation of Galerkin and Petrov-Galerkin model reduction for finite element approximations of the shallow water equations. *Computer Methods in Applied Mechanics and Engineering*. 2017;318:537 - 571.
- [35] Stefanescu R., Navon I.M.. POD/DEIM nonlinear model order reduction of an ADI implicit shallow water equations model. *Journal of Computational Physics*. 2013;237:95 - 114.
- [36] Ștefanescu Răzvan, Sandu Adrian, Navon Ionel M.. Comparison of POD reduced order strategies for the nonlinear 2D shallow water equations. *International Journal for Numerical Methods in Fluids*. 2014;76(8):497-521.
- [37] Bistrian D. A., Navon I. M.. An improved algorithm for the shallow water equations model reduction: Dynamic Mode Decomposition vs POD. *International Journal for Numerical Methods in Fluids*. 2015;78(9):552-580.
- [38] Bistrian Diana A, Navon Ionel M. The method of dynamic mode decomposition in shallow water and a swirling flow problem. *International Journal for Numerical Methods in Fluids*. 2017;83(1):73–89.
- [39] Esfahanian Vahid, Ashrafi Khosro. Equation-free/Galerkin-free reduced-order modeling of the shallow water equations based on Proper Orthogonal Decomposition. *Journal of Fluids Engineering*. 2009;131(7):071401-071401-13.
- [40] Morrison P. J.. Hamiltonian description of the ideal fluid. *Rev. Mod. Phys.*. 1998;70:467–521.
- [41] Salmon Rick. A general method for conserving energy and potential enstrophy in shallow-water models. *Journal of the Atmospheric Sciences*. 2007;64(2):515-531.
- [42] Lynch Peter. *Hamiltonian methods for geophysical fluid dynamics: An introduction*. 2002.
- [43] Wimmer Golo, Cotter Colin, Bauer Werner. Energy conserving upwinded compatible finite element schemes for the rotating shallow water equations. *arXiv e-prints*. 2019;.
- [44] Eldred Christopher, Dubos Thomas, Kritsikis Evaggelos. A quasi-Hamiltonian discretization of the thermal shallow water equations. *Journal of Computational Physics*. 2019;379:1 - 31.

- [45] Salmon Rick. A general method for conserving quantities related to potential vorticity in numerical models. *Nonlinearity*. 2005;18(5):R1–R16.
- [46] Dahlby Morten, Owren Brynjulf, Yaguchi Takaharu. Preserving multiple first integrals by discrete gradients. *Journal of Physics A: Mathematical and Theoretical*. 2011;44(30):305205.
- [47] Celledoni Elena, McLachlan Robert I., McLaren David I., Owren Brynjulf, Quispel G. R. W.. Discretization of polynomial vector fields by polarization. *Proceedings of the Royal Society of London A: Mathematical, Physical and Engineering Sciences*. 2015;471(2184).
- [48] Kahan William, Li Ren-Chang. Unconventional Schemes for a Class of Ordinary Differential Equations-With Applications to the Korteweg-de Vries Equation. *Journal of Computational Physics*. 1997;134(2):316 - 331.
- [49] Miyatake Yuto. Structure-preserving model reduction for dynamical systems with a first integral. *arXiv e-prints*. ;.
- [50] Taira Kunihiko, Brunton Steven L., Dawson Scott T. M., et al. Modal analysis of fluid flows: an overview. *AIAA Journal*. 2017;55(12):4013-4041.
- [51] Drmač Z., Gugercin S.. A new selection operator for the discrete empirical interpolation method-improved a priori error bound and extensions. *SIAM Journal on Scientific Computing*. 2016;38(2):A631-A648.
- [52] Graham W. R., Peraire J., Tang K. Y.. Optimal control of vortex shedding using low-order models. Part Iopen-loop model development. *International Journal for Numerical Methods in Engineering*. 1999;44(7):945-972.
- [53] Holmes Philip, Lumley John L., Berkooz Gahl, Rowley Clarence W.. *Turbulence, coherent structures, dynamical systems and symmetry*. Cambridge Monographs on MechanicsCambridge University Press, Cambridge; second ed.2012.
- [54] Mahoney Michael W., Drineas Petros. CURmatrix decompositions for improved data analysis. *Proceedings of the National Academy of Sciences*. 2009;106(3):697–702.
- [55] Leva P. d.. *MULTIPROD TOOLBOX, multiple matrix multiplications, with array expansion enabled*. : University of Rome Foro Italico, Rome; 2008.
- [56] Sugibuchi Yuya, Matsuo Takayasu, Sato Shun. Constructing invariant-preserving numerical schemes based on Poisson and Nambu brackets. *JSIAM Letters*. 2018;10:53-56.